The HF Surface Wave Radar WERA. Part I: Statistical Analysis of Recorded Data

Salvatore Maresca, Maria Greco, Fulvio Gini,
Dept. of Information Engineering, University of Pisa, via G. Caruso 16, 56122 Pisa (PI), Italy
{salvatore.maresca, m.greco, f.gini}@iet.unipi.it

Raffaele Grasso, Stefano Coraluppi,
NATO Undersea Research Centre, viale S. Bartolomeo 400, 19126 La Spezia (SP), Italy
{grasso, coraluppi}@nurc.nato.int

Nicolas Thomas
SAS ActiMar, 36 Quai de la Douane, 29200 Brest, France
nicolas.thomas@actimar.fr

***Abstract*—Surface wave (SW) over-the-horizon (OTH) radars are not only widely used for ocean remote sensing, but they can also be exploited in integrated maritime surveillance systems. This paper represents the first part of the description of the statistical and spectral analysis performed on sea backscattered signals recorded by the oceanographic WEllen RAdar (WERA) system. Data were collected on May 13th 2008 in the Bay of Brest, France. The data statistical analysis, after beamforming, shows that for near range cells the signal amplitude fits well the Rayleigh distribution, while for far cells the data show a more pronounced heavy-tailed behavior. The causes can be traced in man-made (i.e. radio communications) and/or natural (i.e. reflections of the transmitted signal through the ionosphere layers, meteor trails) interferences.**

I. INTRODUCTION

Despite microwave radars, high-frequency surface-wave radars (HFSWRs) have the ability to detect targets which fall far beyond the optical horizon and, for this reason, are called OTH systems. They operate by normal line-of-sight propagation in addition to a surface wave propagation mode [1]. These systems are mainly used for remote sensing and for oceanic applications (i.e. current mapping and wave spectra analysis). As a matter of fact, recently even growing interest is attributed to tsunami early warning detection [2]. These radar systems operate both from the coast and on board of ships. This is the case of the Coastal Ocean Dynamics Application Radar (CODAR), developed at NOAA, and WEllen RAdar (WERA), developed at the University of Hamburg. Both of them have been operated by the University of Hamburg in a long series of field experiments both in the Atlantic Ocean and Mediterranean Sea [3], [4].

By exploiting the good conductivity of sea water in the lower HF band (3–15 MHz), low-power HFSWRs, such as WERA, can be successfully used in integrated maritime surveillance systems for detecting vessels, ships and go-fast boats. The final aim is to monitor and protect the so called Exclusive Economic Zones (EEZ), as described in [5], [6].

As said, frequencies in the HF band are comprised between 3 and 30 MHz, with wavelengths varying from 100 to 10 m, respectively. Part of the transmitted HF power propagates along the sea surface following Earth's curvature beyond the horizon. However these signals are strongly attenuated and, as a consequence, their working range is limited even if longer than the optical horizon. The attenuation increases with increasing HF frequencies and decreasing sea-water conductivity [4]. The working range of a HF radar depends not only on the attenuation of the electromagnetic wave during the transmitter-target-receiver path, but also on the scattering strength of the target, atmospheric noise and noise due to radio interference [1].

The contribution of HF sea clutter is produced by specific spectral components of the surface-height wavefield. In fact, if the ocean wave spectrum contains sea wavelengths of the order of magnitude of the radar wavelength, the Bragg scattering theory is applicable. First-order Bragg scattering is due to those ocean waves of half the radar wavelength which travel towards and away from the radar site. The Doppler spectrum of the backscattered signal then contains two lines, corresponding to the phase velocities of the scattered ocean waves. These frequencies often deviate from the theoretically known values in non-moving waters. This phenomenon is attributed to an underlying surface current. The full ocean wave spectrum is due to the second-order scattering which generates side-bands in the HF Doppler spectrum. The basic physics of backscattering of electromagnetic waves were discovered and described by Crombie [7] and Barrick [8]. External interference from natural and man-made sources typically masks the entire range-Doppler (RD) search space and is characterized by a spatial covariance matrix that is time-varying or non-stationary over the coherent processing interval (CPI). This physical phenomenon may arise from a

978-1-4244-5813-4/10/$26.00 ©2010 IEEE

Report Documentation Page

Form Approved
OMB No. 0704-0188

1. REPORT DATE	2. REPORT TYPE	3. DATES COVERED
MAY 2010		**00-00-2010 to 00-00-2010**

4. TITLE AND SUBTITLE	5a. CONTRACT NUMBER
The HF Surface Wave Radar WERA. Part I: Statistical Analysis of Recorded Data	5b. GRANT NUMBER
	5c. PROGRAM ELEMENT NUMBER
6. AUTHOR(S)	5d. PROJECT NUMBER
	5e. TASK NUMBER
	5f. WORK UNIT NUMBER
7. PERFORMING ORGANIZATION NAME(S) AND ADDRESS(ES) **University of Pisa,Dept. of Information Engineering,via G. Caruso 16,56122 Pisa (PI), Italy,**	8. PERFORMING ORGANIZATION REPORT NUMBER
9. SPONSORING/MONITORING AGENCY NAME(S) AND ADDRESS(ES)	10. SPONSOR/MONITOR'S ACRONYM(S)
	11. SPONSOR/MONITOR'S REPORT NUMBER(S)

12. DISTRIBUTION/AVAILABILITY STATEMENT
Approved for public release; distribution unlimited

13. SUPPLEMENTARY NOTES
See also ADM002322. Presented at the 2010 IEEE International Radar Conference (9th) Held in Arlington, Virginia on 10-14 May 2010. Sponsored in part by the Navy.

14. ABSTRACT
Surface wave (SW) over-the-horizon (OTH) radars are not only widely used for ocean remote sensing, but they can also be exploited in integrated maritime surveillance systems. This paper represents the first part of the description of the statistical and spectral analysis performed on sea backscattered signals recorded by the oceanographic WEllen RAdar (WERA) system. Data were collected on May 13th 2008 in the Bay of Brest, France. The data statistical analysis, after beamforming shows that for near range cells the signal amplitude fits well the Rayleigh distribution, while for far cells the data show a more pronounced heavy-tailed behavior. The causes can be traced in man-made (i.e. radio communications) and/or natural (i.e. reflections of the transmitted signal through the ionosphere layers, meteor trails) interferences.

15. SUBJECT TERMS

16. SECURITY CLASSIFICATION OF:			17. LIMITATION OF ABSTRACT	18. NUMBER OF PAGES	19a. NAME OF RESPONSIBLE PERSON
a. REPORT **unclassified**	b. ABSTRACT **unclassified**	c. THIS PAGE **unclassified**	**Same as Report (SAR)**	**6**	

number of causes. For instance, the dynamic properties of the ionospheric layers propagating the HF interference, the variation in geometry between radar receiver and interference sources and the impulsive nature of the sources [9]. Unoccupied HF channels are very difficult to find, especially at night, when the ionosphere is prone to propagate interference at long distances. The space-time characterization and modeling of ionospherically propagated signals can be found in [9]. For this reason, adaptive beamforming (ABF) techniques are strongly recommended in order to suppress such interferences effectively [10].

This paper deals with the statistical analysis of sea clutter using signals received by two concurrently operating WERA systems. In sections II and III we provide a brief overview about WERA and the NURC experiment in the Bay of Brest (France), respectively. In Section IV the statistical analysis of the measured data is described, while conclusions are drawn in Section V, together with some guidelines about ongoing and future work.

II. WERA System Description

WERA uses electromagnetic waves between 6 and 30 MHz [11]. The transmitted electromagnetic wave, vertically polarized, travels along the sea surface beyond the horizon and is backscattered by ocean waves. The transmitter and the receiver are de-coupled by using separate locations for the antennas. This solution allows both the transmitter and the receiver to operate simultaneously. Since the receiver is continuously switched on, we are allowed to pick signals from all over the defined range. In order to maximize the covered area, the antennas should either be installed as close to the water as possible, or on top of a cliff [11]. Two different configurations of receiving antennas can be used according to the particular application. A linear receiving antenna array allows to measure surface current velocities, ocean wave height (spectra) and wind. When the receiver configuration is given by 16 line-aligned antennas, the coverage of the HF radar (field of view) is limited to 120°. If only surface currents are needed, a small four-element square array is instead used. WERA system uses frequency modulated continuous wave (FMCW) chirps. Range resolution varies from 0.3 to 1.5 km and depends on the use of different frequency-modulated signals [11].

III. Experiment Description

Data were collected during the NURC experiment at Brest (Brittany, France), on May 13 2008. The two WERA systems, respectively located at the Bay of Brest, at Brezellec (Latitude 48° 4’ 8’’, Longitude 4° 40’ 0’’) and Garchine (Latitude 48° 30’ 10’’, Longitude 4° 46’ 32’’) are owned by the French Service Hydrographique et Océanographique de la Marine (SHOM) and operated by the company SAS ActiMar. The two radars at Garchine and Brezellec, located parallel to the coast, point towards the true North with an angle of 339° and 20°, respectively. The two WERA systems worked at frequencies comprised between 12.190 and 12.565 MHz. This solution allows the operators to transmit and receive on a free HF channel.

At 00:00 UTC, the first radar, located at Garchine, starts transmitting and receiving data looking at the Atlantic Ocean for a period of 8 minutes and 52 seconds, defined as the system. At 00:10 UTC, the radar at Brezellec is set on and collects its own data, for 8 minutes and 52 seconds again. Starting at 00:20 and 00:30 UTC, the second records are collected by the two WERA systems at Garchine and Brezellec, respectively. This procedure then repeats with radars alternating each other every ten minutes. Concluding, at the end we have 17 data files collected at Brezellec and 18 at Garchine. Data records occur every twenty minutes at each receiver and last for 8 minutes and 52 seconds, for a total of 2048 measurements (corresponding to 532 s) with a chirp duration of 0.26 s, which is suitable for sea surface variability. Note that each receiver is composed of 16 line-aligned antennas. Bandwidth was set to 100 kHz (for a range resolution of 1.5 km). Transmitted power was 30 W. For each chirp, 100 range samples were collected (the maximum range is 150 km).

IV. Statistical Analysis

The analysis of data recorded by the two WERA radars can be divided into two major branches. This paper concerns the first of these two parts and provides a detailed study of the statistical characteristics of HF signals. The second part is instead devoted to the analysis of the spectral features and is instead presented in [12]. Before the statistical analysis, data have been beamformed by means of a simple rectangular window [13]. A different windowing function (i.e. Hamming) has been also considered with the purpose of understanding the effect of different beam-widths and side-lobe levels on the range-azimuth (RA) profile of the received signal.

Before any further processing, a preliminary analysis has been carried out on the data, with the final purpose of evaluating the correct balance between the in-phase (I) and quadrature (Q) signal components. This part has been omitted for brevity but can be found in [14].

A. Non-Gaussianity analysis

When the number of scatterers from a given illuminated surface is large enough, the Central Limit Theorem (CLT) applies. The clutter is then a complex Gaussian process or, alternatively, its amplitude is Rayleigh distributed. For this reason, the first step of our survey consists in studying the probability density functions (PDFs) of both the I and Q components and check whether they are Gaussian distributed.

However, instead of proceeding with an extensive comparison of the empiric PDFs, two parameters have been evaluated. By simply calculating the skewness and excess kurtosis coefficients [14] we can describe how a given random real-valued variable deviates from being Gaussian distributed. By denoting with Z the aforementioned generic random variable, they are defined as:

$$\gamma_3(Z) \triangleq \frac{E\left\{\left(Z - E\{Z\}\right)^3\right\}}{E^{3/2}\left\{\left(Z - E\{Z\}\right)^2\right\}}, \qquad (1)$$

$$\gamma_4(Z) \triangleq \frac{E\left\{\left(Z-E\{Z\}\right)^4\right\}}{E^2\left\{\left(Z-E\{Z\}\right)^2\right\}} - 3 . \quad (2)$$

The first parameter provides information about the symmetry of the PDF around its mean value. A negative (positive) value corresponds to a distribution with an asymmetric tail extending to the left (right) of the mean value. Excess kurtosis measures instead the relative peakedness (if negative) or flatness (if positive) of the distribution relative to the Gaussian PDF. For a Gaussian distribution, these parameters are both equal to zero [15].

In this paper we describe only the results obtained by processing the data recorded at Brezellec at 02:30 UTC (corresponding to dataset no. 8) as representative of the results relating to all the files. Values close to zero suggest that the real and imaginary components are likely to be Gaussian-distributed and, as a consequence, the amplitude of a complex-valued random process, with both I and Q Gaussian components, is Rayleigh distributed. Results concerning the excess kurtosis parameter are shown in Fig.1 and describe its behavior in the RA space. For brevity, only the I signal component is shown. As we can observe, its values are close to zero for the majority of RA cells. Significant deviations from the expected Gaussian model can be recognized approximately between 0° and 30° from the broadside direction and starting from range cell (RC) 75. They manifest by means of peak-like values, which can be significantly higher than zero. Similar observations can be drawn from the analysis of the angles between -20° and -5°. In addition, negative values are representative of mixed sea/land cells [14]. If we adopt a different windowing function, e.g. Hamming, sensible differences can be observed in the RA profile of skewness and excess kurtosis. Hamming window reduces side-lobes by 40 dB. As a consequence, some peaks that appear in Fig. 1, due to the high side-lobes in the beam pattern, would be partially eliminated. Conversely, the Hamming window enlarges the main lobe, thus spreading the true peaks over a wider azimuth space.

We can conclude that, for a certain number of RA cells, sea clutter amplitude strongly deviates from the expected Rayleigh density. This is true mostly for long-range cells where unwanted ionospheric propagation modes and/or meteor trail reflections are likely to happen. However, although ionospheric noise negatively affects only distant RCs, it is not the only interference source we must deal with. Radio frequency interference (RFI) is able to mask sea clutter signal (and consequently also targets) in large regions of the RA space. By analyzing the RA non-Gaussianity profile (i.e. skewness and excess kurtosis) of both the I and Q components, we are able to distinguish between the two types, thanks also to their well-defined spectral characteristics, as described in [12].

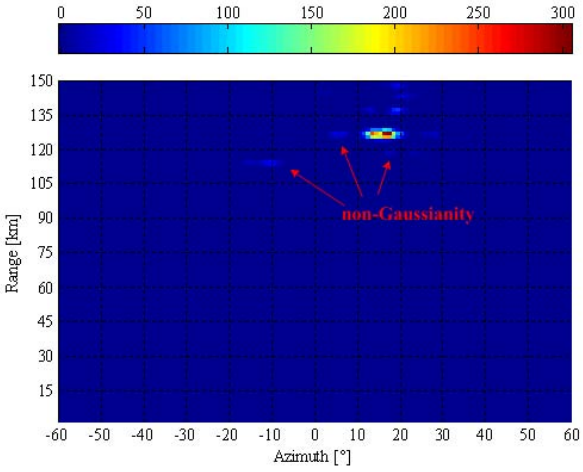

Figure 1. Excess kurtosis vs. RA, I signal component.

B. *Amplitude modeling*

The second step of our analysis consists in evaluating the empirical amplitude distribution and in comparing it with a series of well-known models. These models are commonly used to model the amplitude PDF (APDF) of heavy-tailed non Gaussian X-band sea clutter [15] but can be successfully applied to HF data as well [14]. They are the Rayleigh (R), Log-normal (LN), Weibull (W), and K models. The analytical expressions of these PDFs and their moments are reported below for completeness. Note that with R we denote the clutter amplitude.

Rayleigh (R) model

The expressions of the Rayleigh distribution and its moments are given by:

$$p_R(r) = \frac{2r}{\lambda^2}\exp\left\{-(r/\lambda)^2\right\}u(r) \quad (3)$$

$$E\left\{R^n\right\} = \lambda^n \cdot \Gamma(n/2+1) , \quad (4)$$

where λ is the scale parameter.

Weibull (W) model

$$p_R(r) = \frac{c}{b^c} r^{c-1} \exp\left\{-(r/b)^c\right\}u(r) \quad (5)$$

$$E\left\{R^n\right\} = b^n \cdot \Gamma(n/c+1) , \quad (6)$$

where c is the shape parameter, b is the scale parameter and $\Gamma(x)$ is the gamma function with input argument x. It is worth of note that the Weibull clutter model coincides with the Rayleigh model when $c = 2$.

K-distribution (K) model

$$p_R(r) = \frac{\sqrt{2\nu/\mu}}{2^{\nu-1}\Gamma(\nu)}\left(\sqrt{2\nu/\mu}\cdot r\right)^{\nu} K_{\nu-1}\left(\sqrt{2\nu/\mu}\cdot r\right)u(r) \quad (7)$$

$$E\{R^n\} = \left(\frac{2\mu}{\nu}\right)^{n/2} \frac{\Gamma(\nu+n/2)\Gamma(1+n/2)}{\Gamma(\nu)}, \quad (8)$$

where ν is the shape parameter and μ is the scale parameter. Function $K_{\nu-1}(y)$ is the modified Bessel function of the third kind of order $\nu-1$ with input arguments y. It is worth of note that the K clutter model tends to the Rayleigh model when ν increases ($\nu > 10$ in practice means Gaussian clutter, i.e. Rayleigh APDF).

Log-normal (LN) model

$$p_R(r) = \frac{1}{r\sqrt{2\pi\sigma^2}} \exp\left\{-\frac{1}{2\sigma^2}\left[(\ln r - \ln\delta)^2\right]\right\} u(r) \quad (9)$$

$$E\{R^n\} = \delta^n \exp\{n^2\sigma^2/2\}, \quad (10)$$

where σ is the shape parameter, δ is the scale parameter and $u(r)$ is the unit step function.

The characteristic parameters of the theoretical distributions have been estimated by the method of moments (MoM) [15]. The analysis of both APDF and normalized moments has been carried out for different RA cells. The results of our analysis show that the best fitting is obtained with the Weibull model, as shown in Fig. 2 for RC 74 (extending from 109.5 to 111 km) and the azimuth angle of 0°. Anyway, the differences between the Rayleigh (red line) and Weibull (green line) APDFs are very small, since $\hat{c} \cong 2$. Concluding, the Rayleigh model is a good compromise between model simplicity and model accuracy, although the Weibull model demonstrates the best one, especially for mixed sea/land RA cells, for which $\hat{c} > 2$ [14].

However, as well known, HF signals suffer from a variety of interference sources, both man-made (i.e. radio communications) and natural (i.e. lightning, meteor trails, signal propagation modes through the ionosphere layers).

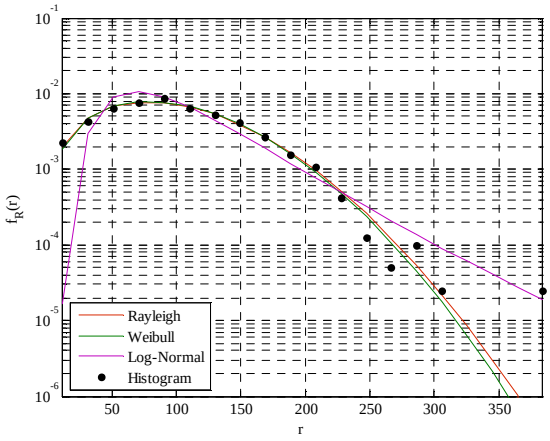

Figure 2. Amplitude PDF for RC 74 and azimuth 0°.

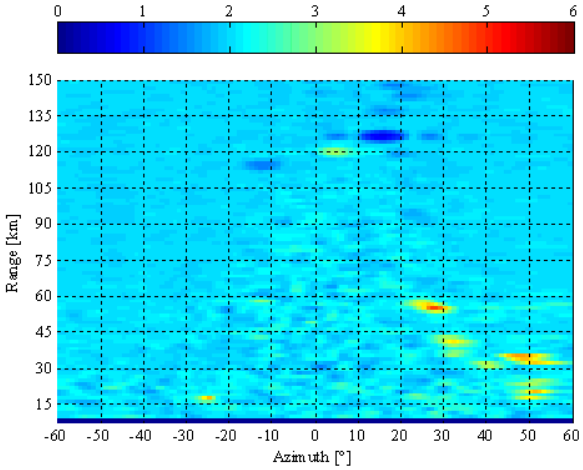

Figure 3. Weibull shape parameter vs RA.

They strongly influence the clutter amplitude density, as demonstrated by the analysis of both the excess kurtosis (i.e. $\hat{\gamma}_4 \gg 0$) and the Weibull shape parameter (i.e. $\hat{c} < 2$), as shown in figures 1 and 3 respectively. The huge peaks traduce in heavy-tailed densities we are unable to describe with the most common sea clutter models [15], even if we consider two generalized K (GK) models, belonging to the compound-Gaussian (CG) family. The expression of their APDF and moments is provided afterwards.

Generalized K (GK) with log-normal (LN) texture

$$p_R(r) = \frac{r}{\sqrt{2\pi\sigma^2}} \cdot \int_0^\infty \frac{2}{\tau^2} \cdot \exp\left\{\frac{r^2}{\tau} - \frac{1}{2\sigma^2}\left[\ln\left(\frac{\tau}{2m}\right)\right]^2\right\} \cdot d\tau \quad (11)$$

$$E\{R^n\} = (2m)^{n/2} \cdot \Gamma\left(1+\frac{n}{2}\right) \cdot \exp\left(\frac{n^2\sigma^2}{8}\right) \quad (12)$$

where σ is the shape parameter and m is the scale parameter of the LN distribution.

Generalized K (GK) with generalized gamma texture

The expression of the APDF of a GK distribution with generalized gamma texture is:

$$p_R(r) = \frac{2br}{\Gamma(\nu)} \cdot \left(\frac{\nu}{\mu}\right)^{\nu b} \cdot \int_0^\infty \tau^{\nu b-2} \cdot \exp\left\{\frac{r^2}{\tau} - \left(\frac{\nu}{\mu}\tau\right)^b\right\} \cdot d\tau \quad (13)$$

$$E\{R^n\} = \left(\frac{\mu}{\nu}\right)^{n/2} \cdot \frac{\Gamma(\nu+n/2b) \cdot \Gamma(1+n/2)}{\Gamma(\nu)} \quad (14)$$

A simple case is reported in Fig. 4 for range cell 76 and for an azimuth angle of -11°, for which the tail of the estimated density extends over those of the proposed models. It is worth noting that the first part of the density (i.e. the "bell") remains similar to the Rayleigh one, while the tail is generally very

long. As demonstrated by the analysis of the amplitude history of the signal in Fig. 5, for the most part of the time we are not able to appreciate any significant variations in the signal amplitude. The strong peak which occurs slightly after 200 s is probably caused by a direct reflection of the transmitted HF signal against a meteor trail.

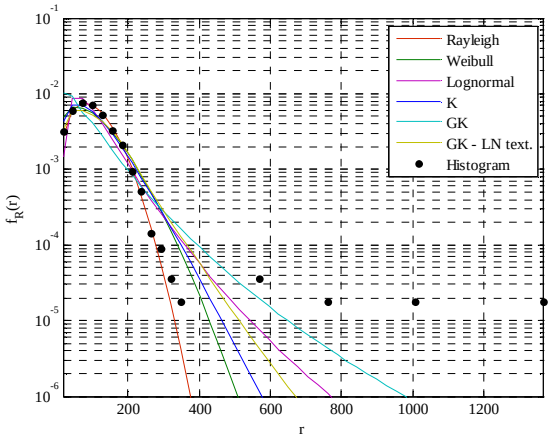

Figure 4. Amplitude PDF for RC 76 and azimuth -11°.

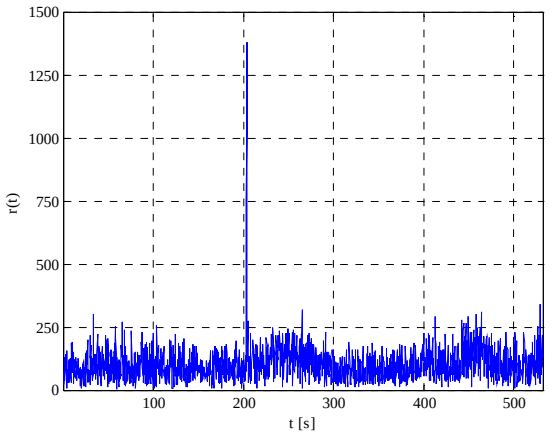

Figure 5. Amplitude history for range cell 76 and azimuth -11°.

Summing up, the shape parameter of the Weibull distribution has been evaluated for all the RA cells, as reported in Fig. 3. It provides useful information about what the radar is observing. For the majority of cells, values are close to 2, thus allowing us to state that the clutter is Rayleigh distributed. The shape parameter is greater than 2 for mixed/land cells and smaller than 2 for interference-corrupted RA cells. These cells are characterized by a heavy-tailed distribution that can still be modeled with a compound Gaussian (CG) distribution (note that the Rayleigh, Weibull and K are CG models) even for long-range cells.

C. Validation of the compound-Gaussian model

Formally a discrete-time compound-Gaussian process can be represented as in [16]. According to this model, the amplitude $r(n)$ of the received complex samples $z(n)$ can be written as follows:

$$r(n) \triangleq |z(n)| = \sqrt{\tau(n)} \cdot |x(n)|, \tag{15}$$

where $x(n)$ is the complex Gaussian random process that accounts for the local sea back-scattering process (speckle), while $\tau(n)$ is a slowly varying non-negative process (texture) that introduces a power modulation of the speckle. Since $\tau(n)$ is appreciably slowly varying with respect to $x(n)$, on a proper time slot denoted with L_c and called coherence time, $z(n)$ can be represented as the product of a random constant times a Gaussian process, i.e.:

$$z(n) = \sqrt{\tau(l)} \cdot x(n), \tag{16}$$

with $n = l - L_c/2, ..., l + L_c/2 - 1$. In the analysis of the sea clutter it is important to validate its compound nature and to measure the coherence length of the texture. A measurement procedure for calculating it is the following. According to (16), we can estimate the texture sequence as follows:

$$\hat{\tau}(l) = \frac{1}{L_c} \cdot \sum_{k=l-L_c/2}^{l+L_c/2-1} |z(k)|^2 . \tag{17}$$

A statistical composite test was proposed to estimate the coherence time length, [16]. However it has a drawback in the need of correctly defining a threshold for each specific significance level. Here a different approach has been chosen. For each possible coherence length it is possible to use equation (17) and the following equation to obtain the estimate of the speckle sequence:

$$\hat{x}(n) = \frac{z(n)}{\sqrt{\hat{\tau}(n)}} . \tag{18}$$

Let $\hat{x}(n \mid L_c)$ be the complex-valued speckle sequence for the hypothetical coherence length L_c. Testing whether the coherence time is at least L_c is related to verify if the real and imaginary parts of the speckle are both Gaussian-distributed. A convenient option to measure the departure from Gaussian statistics is the Jarque-Bera (JB) test, which is based on the estimation of the sample skewness and excess kurtosis of the speckle process [17]. It has the form:

$$JB = \frac{N_S}{6} \cdot \left[\gamma_3^2 + \frac{\gamma_4^2}{4} \right] \tag{19}$$

where N_S, is the number of available observations, while γ_3 and γ_4 are the sample skewness and kurtosis respectively. Once estimated the speckle and texture time sequences, our aim is to compare their APDF and PDF with the Rayleigh model and the other PDFs. This task is accomplished once we have estimated the coherence length of the texture process. Results are shown in Fig. 6 for RC 85 and azimuth 15°. This RA cell is characterized by the presence of a strong non-

Gaussianity, corroborated by the concurrent analysis of figures 1 and 3. We observe that the coherence time is about 40, corresponding to 10.4 s. However, the estimated L_c depends on the type of interference source and strongly decreases with increasing distance. Simulation results demonstrated that $20 < \hat{L}_c < 50$ for ionospheric noise and instead $10 < \hat{L}_c < 20$ for RFI, in strongly dependence on the impulsive nature of sources. Finally, the resulting amplitude of the speckle sequence is Rayleigh-distributed, as shown in Fig. 7.

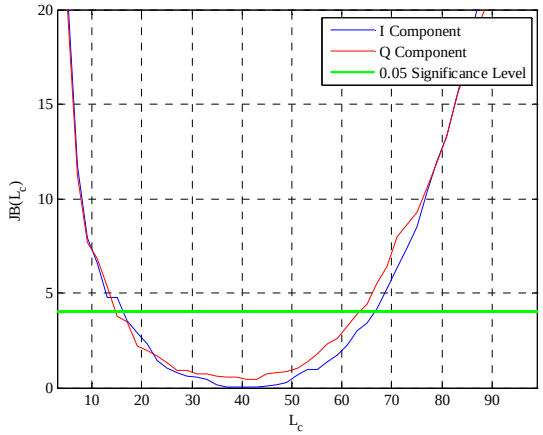

Figure 6. Jarque-Bera test for RC 85 and azimuth 15°.

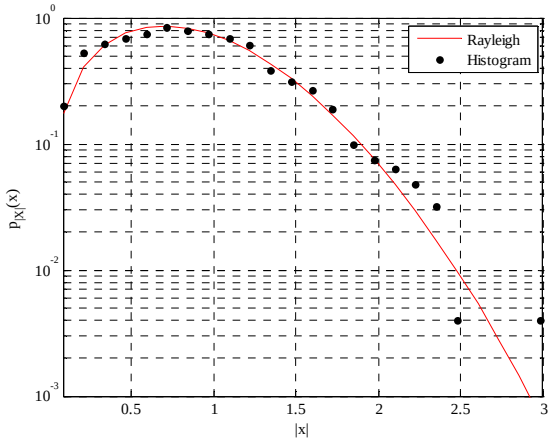

Figure 7. Speckle APDF for RC 85 and azimuth 15°.

V. CONCLUSIONS

A detailed study of the statistical properties of sea clutter in the HF band has been presented. Results show that sea clutter in the HF band can be modeled as a complex Gaussian process, when no interference signals are present. However, mixed sea/land cells are best described by the Weibull model. No optimum fit was found for interference-corrupted cells. For these cells, the validation of the CG model has been addressed, concluding that the CG model is a good candidate even if different interference sources are described by different coherence time lengths of the texture sequence.

REFERENCES

[1] J. M. Headrick, and M. I. Skolnik, "Over-the-Horizon Radar in the HF Band," *Proceedings of the IEEE*, vol. 62, no. 6, pp. 664-673, June 1974.

[2] A. Dzvonkovskaya, K. W. Gurgel, T. Pohlmann, T. Schlick, J. Xu, "Simulation of Tsunami Signatures in Ocean Surface Current Maps Measured by HF Radar," *Proceedings of Oceans 2009*, Bremen, Germany, May 2009.

[3] K. W. Gurgel, G. Antonischki, H. H. Essen, and T. Schlick, "Wellen Radar (WERA): a new ground-wave radar for ocean remote sensing," Coastal Engineering, vol. 37, no. 3, pp. 219-234, August 1999.

[4] K. W. Gurgel, H. H. Essen, and S. P. Kingsley, "High-frequency radars: physical limitations and recent developments," Coastal Engineering, vol. 37, no. 3, pp. 201-218, August 1999.

[5] A. M. Ponsford, L. Sevgi, and H. C. Chan, "An Integrated Maritime Surveillance System Based on High-Frequency Surface Wave radars. Part 2: Operational Status and System Performance," IEEE Antennas and Propagation Magazine, vol. 43, no. 5, pp. 52-63, October 2001.

[6] A. M. Ponsford, "Surveillance of the 200 Nautical Mile Exclusive Economic Zone (EEZ) Using High Frequency Surface Wave Radar (HFSWR)," *Canadian Journal on Remote Sensing*, vol. 27, no. 4, Special Issue on Ship Detection in Coastal Waters, pp. 354-360, August 2001.

[7] D. D. Crombie, "Doppler Spectrum of Sea Echo at 13.56 Mc/s," Nature 175, pp. 681-682, 1955.

[8] D. E. Barrick, "First-Order Theory and Analysis of MF/HF/VHF Scatter from the Sea," *IEEE Transactions on Antennas and Propagation*, vol. 20, no.1, pp. 2-10, January 1972.

[9] G. A. Fabrizio, "Space-Time Characterisation and Adaptive Processing of Ionospherically-Propagated HF Signals," Doctoral Philosophy Thesis Dissertation, July 2000.

[10] G. A. Fabrizio, A. B. Gershman, and M. D. Turley, "Robust Adaptive Beamforming for HF Surface Wave Over-The-Horizon Radar," *IEEE Transactions on Aerospace and Electronic Systems*, vol. 40, no. 2, pp. 510-525, April 2004.

[11] http://ifmaxp1.ifm.zmaw.de/WERA.shtml

[12] S. Maresca, M. Greco, F. Gini, R. Grasso, S. Coraluppi, and N. Thomas, "The HF Surface Wave Radar WERA. Part II: Spectral Anlaysis of Recorded Data," submitted to the *IEEE Radar Conference 2010*, Washington DC, USA, May 2010.

[13] P: Stoica, R. Moses, Spectral Analysis of Signals, "Beamforming and Array Processing," Pearson Prentice Hall 2005.

[14] M. Greco, S. Maresca, F. Gini, R. Grasso, and S. Coraluppi, "Statistical Analysis Measured by the HF Surface Wave Radar WERA," *NATO Workshop on Data Fusion and Anomaly Detection for Maritime Situation Awareness*, La Spezia, Italy, Septmeber 2009.

[15] M. Greco, F. Gini, and M. Rangaswamy, "Statistical Analysis of Measured Polarimetric Clutter Data at Different Range Resolutions," IEE Proceedings on Radar, Sonar Navigation, vol. 153, no. 6, pp. 473-481, December 2006.

[16] E. Conte, M. Di Bisceglie, C. Galdi and G. Ricci, "A Procedure for Measuring the Coherence Length of the Sea Texture," IEEE Transactions on Instrumentation and Measurement, vol. 46, no. 4, pp. 836-841, August 1997.

[17] A. K. B. Carlos M. Jarque, "Efficient tests for Normality, Homoscedasticity and Serial Independence of Regression Residuals," Economic Letters, vol. 6, no. 3, pp. 255-259, October 1980.